ISSN 8756-6990, Optoelectronics, Instrumentation and Data Processing, 2019, Vol. 55, No. 3, pp. 263–270. © Allerton Press, Inc., 2019.
Russian Text © The Author(s), 2019, published in Avtometriya, 2019, Vol. 55, No. 3, pp. 62–70.

ANALYSIS AND SYNTHESIS OF SIGNALS AND IMAGES

Neural Network Classification of Difficult-to-Distinguish Types of Vegetation on the Basis of Hyperspectral Features

E. S. Nezhevenko*

Institute of Automation and Electrometry, Siberian Branch, Russian Academy of Sciences, pr. Akademika Koptyuga 1, Novosibirsk, 630090 Russia
**E-mail: nejevenko@ iae.nsk.su*

Received April 29, 2019; revision received May 7, 2019; accepted for publication May 7, 2019

Abstract—It is experimentally demonstrated that the classification of fragments of a hyperspectral image with preliminary transformation of the spectral features of the image into the principal components and with the use of the Hilbert–Huang spectral transform is fairly effective in the case of vegetation types that are difficult-to-distinguish on the basis of hyperspectra. This classification is compared with traditional methods, where hyperspectral features transformed to the principal components without using spatial information are used. RBF neural networks are used in all methods at the final stage of the classification.

Keywords: classification, hyperspectral image, Hilbert–Huang transform, principal components, neural networks.

DOI: 10.3103/S8756699019030087

INTRODUCTION

There has been significant recent progress in solving an important problem of classifying terrain images on the basis of their hyperspectral images (HSIs) [1, 2]. Investigations validated by HSI experiments were described in [3–7]. Various aspects of this problem were considered; the main point was demonstration of the fact that a significant increase in the percentage of correct HSI classification is ensured by taking into account the spatial structure. The cycle of investigations [5–7] was finalized by the review paper [8]. It is of interest to cite the conclusion made in [7]: "It is reasonable to apply further efforts in this field to the development of classification algorithms that can improve the efficiency of distinguishing similarly looking types of vegetation..."

The goal of the present study is to demonstrate that the method tested by an example of a small-size HSI fragment [9] successfully solves the problem, which was only outlined in [8]. At the same time, this method applied to a HSI fragment 145×145 pixels with 15 classes (this image was used in [5–7]) provided 99.1% of correct classification for the test sample and 99.7% for the learning sample, which is more than convincing as compared to other methods.

CHARACTERISTIC OF THE CLASSIFIED OBJECT

For comparisons of different classification methods, it is important that objects used in experiments should be similar to each other (the best option is to use identical objects). The object called Lena was used in many experiments including image processing [10]. In the case of HSI processing, the image obtained within the Airborne Visible Infrared Imaging Spectrometer (AVIRIS) program at the Indian Pines test field (Indiana, USA) was taken as a reference object. The image size was 614×2677 pixels, the resolution was 20 m/pixel, and the number of channels was 220 in the range from 0.4 to 2.5 μm. On the basis of on-ground observations, the image was divided into 58 classes, including 15 classes of corn and 18 classes of soya produced by different methods. Let us recall the citation from Introduction. In [6, 7], all classes of corn

and soya were united into two classes in the HSI analysis. The reason for this unification was not explained, but it can be assumed that the percentage of correct classification would have drastically decrease if this unification were not used. Let us find the reason for this problem. Obviously, the spectral characteristics of all regions of corn or soya growing are similar. Therefore, the difference between such objects can be increased only by using spatial features. A large number of spatial processing algorithms were analyzed in [8]; most of them are based on allocation of the pixel value by means of processing of its neighborhood. However, the properties of the processed structures are ignored, and fine differences are not detected. In [9], the principal components (PCs) of the HSI were divided into internal oscillations (empirical modes). As a result, features determined by the internal structure of this or that fragment were identified, which allowed fine differences between the structures to be found.

STAGES OF PROCESSING

For experimental verification of the possibility of fine classification, a fragment 580×580 pixels from the 1378th to the 1957th pixel in the vertical direction and from the 0th to the 579th pixel in the horizontal direction (Fig. 1a) is cut out from the above-described HSI (the algorithm processes square fragments, and a sufficiently informative fragment is chosen). It contains regions including 44 classes (let us recall that the entire test field was divided into 58 classes). Division of the fragment into classes in pseudo-colors is shown in Fig. 1b.

Each pixel of the fragment is characterized by 200 spectral components (in fact, the number of spectral components is 220, but 20 most noisy components are not used for processing), which are mutually correlated to a large extent. Therefore, they are transformed to the PCs, and five PCs including 99.42% of data dispersion are chosen for processing. Each PC is expanded into five empirical modes (the so-called Huang transform). As this algorithm was described in sufficient detail in [9], only brief information is provided here.

The algorithm of expansion of the one-dimensional signal function into empirical modes (EMs) looks as follows. Local extreme (minimum and maximum) points of the signal are determined. Approximating local maximums and local minimums separately, we obtain the signal envelopes. Thus, we have the function $h_1 = x(t) - m_1$, where m_1 is the mean value of the upper and lower envelopes, and $x(t)$ is the signal. Then the function h_1 is taken as the initial signal, and the algorithm is applied again until the threshold condition is satisfied. To check this condition, we calculate the normalized squared difference between two consecutive sieving operations. If $\mathrm{SD}_k < \delta$, then the sieving process is stopped.

After terminating the process at h_k, we take the function c_1 as the first EM. As the initial signal r_1, we take the difference $x(t) - c_1$, and the process is repeated. Finally, we obtain the expansion of the signal into the EMs:

$$x(t) = \sum_{j=1}^{n} c_j + r_n.$$

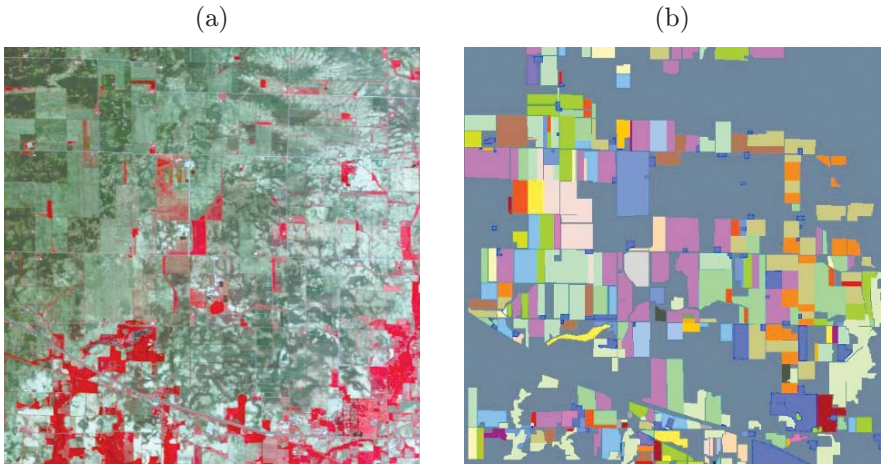

Fig. 1.

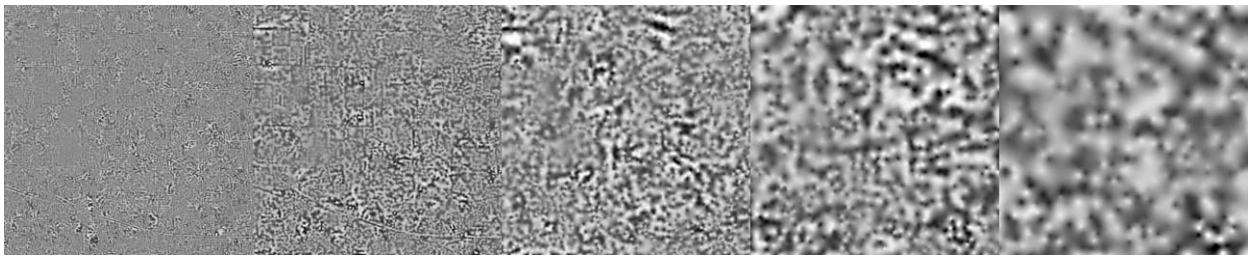

Fig. 2.

The algorithm of expansion of the two-dimensional signal into EMs is formally the same as that used for one-dimensional signal expansion. In this case, however, it is necessary to solve a number of problems; the main problem is to find local extreme points and construct the signal envelope on the basis of these points. In the two-dimensional case, the neighborhoods of local extreme points are not always determined uniquely. To avoid this problem, we use morphological reconstruction [11] based on geodesic operators for finding the local minimums and maximums. The geodesic reconstruction can be defined as iterative repetition of geodesic dilatation until no more image changes are observed. Thus, geodesic dilatation is used to find the maximums in the image, and geodesic erosion is applied to find the minimums in the image. The method of determining the minimum and maximum points was described in [12].

Cubic splines are usually used to construct the envelopes in the one-dimensional case. For two-dimensional images, however, interpolation by cubic splines yields intense perturbations at the image edges. Carr et al. [13] proposed to use radial basis functions (RBFs) for interpolation; these functions can be presented in the form

$$s(x) = p_m(x) + \sum_{i=1}^{N} \lambda_i \Phi(\|x - x_i\|),$$

where s is the radial basis function, p_m is the low-power polynomial, λ is the coefficient, Φ is the basis function, and x_i are the centers of the basis functions. The RBF approximation method offers certain advantages as compared to spline approximation. The centers of the basis functions may be located outside the grid nodes. Moreover, the RBF method is suitable for interpolation of inhomogeneous data. A code in the MATLAB environment was developed for the above-described two-dimensional transform. Each of the four PCs was divided into five EMs. The result of decomposition of the first PC is shown in Fig. 2.

It is seen that the frequency of the structure decreases with an increase in the mode number. Thus, a 20-dimensional vector corresponds to each of the pixels 580×580 in size. Classification of various regions was performed with the use of preliminary trained neural networks. Several types of neural networks were considered: linear network, multilayer perceptron, and RBF networks. The best classification results were obtained with RBF networks. Any classification is the process of finding a set of hypersurfaces that ensure bounding or contouring of sets representing individual classes. This division can be provided by means of describing each of the sets with the use of complete coverage of the space by a certain set of hyperspheres. Neural networks that ensure such classification are called the RBF networks and represent a particular case of direct-propagation two-layer networks. Each element of the hidden layer employs a Gaussian-type RBF as an activation function. It is centered at a point determined by the weight vector related to the neuron. The position and width of the kernel function should be trained on learning samples. However, the number of kernels is usually much smaller than the number of learning examples. There are various algorithms of RBF network learning; one of them is based on a two-stage learning strategy or mixed learning. It estimates the kernel position and width by the clusterization algorithm "without the teacher" first and then by using the algorithm of minimization of the root-mean-square error "with the teacher" for determining the weights of the bonds between the hidden and output layers. When this initial approximation is obtained, the gradient descent is applied to refine the network parameters. The number of input neurons of the RBF network is equal to the number of recognition features, the number of output neurons is equal to the number of classes, and the number of elements in the hidden layer is determined in the course of learning.

Table 1. Results of classification for 44 classes

Network architecture / system of features	Classification accuracy		
	learning sample	control sample	test sample
RBF 5-700-44 / PC	0.525	0.503	0.495
RBF 20-1500-44 / EMPC	0.792	0.712	0.679

RESULTS OF THE EXPERIMENT (FOR ALL CLASSES)

The basic analysis was performed for similarly looking classes. However, to compare the method proposed in the present paper with other available methods (in particular, those described in [8]), we describe the results of classification for all 44 classes in the chosen region. Each region was divided into three samples: learning, control, and test samples in the ratio 50 : 25 : 25%, and the best RBF network from the viewpoint of correct classification was chosen from a set of ten trained RBF networks. The results of the analysis performed on the principal components without their transformation to empirical modes are summarized in the first row of Table 1.

The first column of Table 1 provide information about the neural network architecture: network type, number of input neurons, number of RBFs in the hidden layer, and number of output neurons. Obviously, the classification accuracy of 49.5% cannot be considered as satisfactory. Let us now consider the results of learning, i.e., classification on data first transformed to principal components and then each chosen PC is expanded into EMs, from which recognition features are determined (this is the Hilbert–Huang transform). The results of such processing are presented in the second row of Table 1.

The total accuracy of the classification of the test sample is 67.9%, i.e., it increases by 18.4% owing to spatial processing, which can be considered as a good result in view of the fact that all regions of corn and soya were classified separately. However, the main experiment was aimed at classification of different variants of the corn and soya regions.

EXPERIMENTAL RESULTS (FOR THE CORN AND SOYA CLASSES)

The chosen fragment 580×580 pixels in size contains 11 corn regions and 15 soya regions — a total of 26 regions out of 36. First we show the results of models for classification of the corn and soya regions in terms of the principal components without spatial processing (first row in Table 2).

The classification accuracy equal to 54% is slightly higher than for 44 classes. For the experiment with spatial processing, we formed a file consisting of pixels belonging to 11 classes of corn and 15 classes of soya beans. The file size was 20×105470, where 20 means five PCs and four EMs, and 105470 is the total number of all pixels in the assigned regions. The number of pixels in each class was different, but the proportional division into the learning, test, and control samples was the same (50 : 25 : 25 %). Pixels for all samples were chosen randomly. The learning sample was loaded into the neural network of the RBF type, and the maximum number of elements in the hidden layer was 1500. Learning was performed by means of backpropagation, optimization was performed by the method of adjoint gradients, and the learning time was several hours. The learning procedure was finalized on the basis of the "behavior" of the correct classification of the control sample. Let us analyze the results in more detail, leaving, as previously, the most effective network among ten networks under consideration (second row in Table 2).

The total accuracy of classification of the test sample equal to 88.8% can be considered as sufficiently good. However, it is of interest to consider fine details of discerning regions of the same vegetation into classes with allowance for minor differences between them. All regions included into the chosen fragment are listed in Table 3, where their characteristics are also given.

Their numeration allows one to identify these regions in experimental data. The results of classification with separation into classes are summarized in Table 4.

Table 2. Results of classification of the corn and soya regions in 26 classes

Network architecture / system of features	Classification accuracy		
	learning sample	control sample	test sample
RBF 5-700-26 / PC	0.558	0.528	0.542
RBF 20-1500-26 / EMPC	0.907	0.883	0.888

Table 3. Corn and soya classes

Class number	Vegetation type and characteristics of the region
5	Corn
6	Corn?
7	Corn — west–east
8	Corn — north–south
9	Corn — usual ploughing
12	Corn — usual ploughing — irrigation — north–south
14	Corn — low-intrusive ploughing
15	Corn — low-intrusive ploughing — west–east
16	Corn — low-intrusive ploughing — north–south
17	Corn — no ploughing
18	Corn — no ploughing — west–east
36	Soya beans
38	Soya beans?
39	Soya beans — north–south
41	Soya beans — usual ploughing — west–east
42	Soya beans — usual ploughing — north–south
43	Soya beans — usual ploughing — trench planting
44	Soya beans — weed-covered — usual ploughing
45	Soya beans — trench planting
46	Soya beans — low-intrusive ploughing
47	Soya beans — low-intrusive ploughing — west–east
48	Soya beans — low-intrusive ploughing — trench planting
49	Soya beans — low-intrusive ploughing — north–south
51	Soya beans — no ploughing — west–east
52	Soya beans — no ploughing — north–south
53	Soya beans — no ploughing — trench planting

Table 4. Classification of corn and soya

Class	Total	Correctly	Erroneously	% of correct data	% of erroneous data
5	1582	1350	232	85.34	14.67
6	250	189	61	75.60	24.40
7	1500	1369	131	91.27	8.73
8	6596	6024	572	91.33	8.67
9	12144	11286	858	92.93	7.07
12	1728	1430	298	82.76	17.25
14	4816	4299	517	89.27	10.74
15	5943	5438	505	91.50	8.50
16	1974	1642	332	83.18	16.82
17	960	797	163	83.02	16.98
18	5685	5259	426	92.51	7.49
36	894	767	127	85.79	14.21
38	2124	1538	586	72.41	27.59
39	2726	2270	456	83.27	16.73
41	6042	5188	854	85.87	14.13
42	820	682	138	83.17	16.83
43	543	543	0	100.0	0.00
44	6127	5696	431	92.97	7.03
45	1011	803	208	79.43	20.57
46	1832	1630	202	88.97	11.03
47	2951	2615	336	88.61	11.39
48	2674	2298	376	85.94	14.06
49	1940	1759	181	90.67	9.33
51	929	805	124	86.65	13.35
52	8260	7795	465	94.37	5.63
53	583	575	8	98.63	1.37

Table 5. Normalized matrix of errors of corn and soya classification into 26 classes expressed in percent

N	5	6	7	8	9	12	14	15	16	17	18	36	38	39	41	42	43	44	45	46	47	48	49	51	52	53
5	**100**	0.00	0.00	0.30	1.41	0.00	0.15	0.07	0.07	0.00	0.00	0.00	0.00	0.00	0.00	0.00	0.00	0.07	0.00	2.81	0.00	1.04	0.00	0.00	0.00	0.00
6	0.00	**100**	0.00	0.00	0.00	0.00	0.00	0.00	0.00	0.00	0.00	0.00	0.00	0.00	3.17	0.00	0.00	0.00	0.00	0.00	0.00	0.00	0.00	0.00	0.00	0.00
7	0.58	0.22	**100**	0.29	0.29	0.00	0.29	0.00	0.07	0.00	0.00	0.00	0.22	0.00	0.07	0.00	0.00	0.00	0.00	0.00	0.22	0.00	0.00	0.00	0.00	0.00
8	0.07	0.00	0.05	**100**	1.78	1.13	0.85	0.88	0.08	0.15	0.78	0.12	0.71	0.40	1.61	1.34	0.00	1.44	0.43	0.05	0.58	0.27	0.28	0.03	1.15	0.00
9	0.66	0.39	0.45	1.42	**100**	0.67	1.84	0.69	0.77	0.44	0.90	0.33	1.05	1.22	2.53	0.24	0.00	0.85	0.15	0.58	0.74	0.23	0.62	0.02	0.77	0.04
12	0.00	0.00	0.21	0.70	0.98	**100**	0.91	0.14	0.00	0.00	0.00	0.00	0.07	0.49	0.42	0.00	0.00	0.00	0.00	0.00	0.00	0.14	0.00	0.00	0.00	0.00
14	0.65	0.28	0.00	0.42	1.54	0.07	**100**	0.70	0.51	0.16	0.12	0.00	0.54	0.44	0.98	0.00	0.00	0.67	0.07	1.02	0.16	0.98	0.19	0.02	0.33	0.00
15	0.07	0.00	0.07	0.57	0.72	0.24	0.64	**100**	0.35	0.07	0.24	0.04	1.18	0.42	1.27	0.02	0.00	0.70	0.07	0.00	0.51	0.86	0.29	0.37	0.88	0.00
16	0.00	0.00	0.06	0.24	0.12	0.00	0.00	0.00	**100**	0.00	0.85	0.00	0.24	0.00	0.00	0.00	0.00	0.18	0.37	0.00	0.43	0.12	0.00	0.00	0.73	0.00
17	0.00	0.00	0.00	2.38	0.88	0.00	0.13	0.50	0.25	**100**	0.00	0.00	0.00	0.38	0.00	0.00	0.00	1.51	0.00	0.00	0.75	0.00	0.00	0.00	0.38	0.00
18	0.08	0.00	0.23	0.97	0.74	0.40	0.21	0.63	0.82	0.00	**100**	0.00	1.08	0.21	0.44	0.34	0.00	0.48	0.36	0.00	0.36	0.61	0.06	0.49	1.24	0.00
36	0.26	0.00	0.00	0.00	3.65	0.00	0.26	0.00	0.00	0.00	0.00	**100**	0.00	0.00	0.13	0.00	0.00	0.00	0.00	0.00	0.00	0.78	0.00	0.00	0.00	0.00
38	0.06	0.00	0.84	1.75	1.10	0.06	0.52	0.32	0.13	0.06	0.00	0.00	**100**	0.91	0.71	0.00	0.00	0.26	0.00	0.00	0.06	0.00	0.13	0.00	1.49	0.00
39	0.04	0.00	0.13	0.79	1.28	0.97	0.09	0.48	0.04	0.18	0.48	0.00	0.48	**100**	0.57	0.00	0.00	1.19	0.00	0.00	0.70	0.13	0.09	0.00	0.09	0.00
41	0.06	0.00	0.31	0.94	2.72	0.29	1.10	1.21	0.17	0.40	0.42	0.06	1.08	1.81	**100**	0.02	0.00	0.42	0.21	0.10	0.25	1.20	0.08	0.06	0.35	0.02
42	0.00	0.00	0.00	1.17	0.00	0.00	0.29	0.00	0.15	0.00	0.00	0.00	1.17	1.17	0.73	**100**	0.00	0.29	0.00	0.00	0.15	0.15	0.00	0.00	0.00	0.00
43	0.00	0.00	0.00	0.00	0.18	0.00	0.00	0.00	0.00	0.00	0.00	0.00	0.00	0.00	0.00	0.00	**100**	0.00	0.00	0.00	0.00	0.00	0.00	0.00	0.92	0.00
44	0.09	0.00	0.16	1.33	2.35	0.30	0.46	0.42	0.53	0.40	0.68	0.23	0.88	0.95	2.02	0.02	0.00	**100**	0.23	0.19	0.84	0.51	0.46	0.00	1.39	0.04
45	0.00	0.00	0.00	0.00	0.37	0.00	0.00	0.00	4.86	0.00	0.00	0.00	0.00	0.00	0.12	0.00	0.00	0.12	**100**	0.00	0.00	0.12	0.00	0.00	0.12	0.00
46	1.90	0.00	0.00	0.18	0.67	0.00	0.80	0.06	0.06	0.00	0.00	0.00	0.12	0.06	0.55	0.00	0.00	0.00	0.00	**100**	0.06	0.18	0.00	0.06	0.00	0.00
47	0.80	0.08	0.08	0.19	0.73	0.23	0.15	1.53	0.23	0.04	0.27	0.00	0.61	1.11	0.27	0.00	0.00	0.80	0.80	0.15	**100**	1.07	0.00	0.38	1.11	0.00
48	0.26	0.00	0.57	1.04	1.13	2.05	0.35	0.70	0.13	0.00	0.39	2.09	0.26	0.13	0.70	0.00	0.00	0.04	0.00	0.00	0.13	**100**	0.00	0.87	0.39	0.00
49	0.11	0.00	0.00	0.00	0.85	0.11	0.00	0.85	0.63	0.63	1.88	0.00	0.00	0.00	0.57	0.00	0.00	0.28	2.33	0.06	0.11	0.17	**100**	0.00	0.00	0.00
51	0.00	0.00	0.00	0.00	0.00	0.00	1.12	2.8	0.00	0.00	0.00	0.00	0.00	0.00	0.00	0.00	0.00	0.00	0.00	0.00	0.99	0.00	0.00	**100**	0.12	0.00
52	0.47	0.00	0.01	0.76	1.72	0.09	0.77	1.35	0.63	0.41	1.55	0.22	1.58	0.36	1.68	0.12	0.00	0.72	0.60	0.38	0.69	0.74	0.42	0.50	**100**	0.01
53	0.00	0.00	0.00	0.35	0.52	0.00	0.17	0.00	0.00	0.00	0.52	0.00	0.00	0.00	0.87	0.00	0.00	0.17	0.00	0.00	0.00	0.17	0.00	0.00	0.00	**100**

It is seen that they are significantly nonuniform: 100% correct classification of class 43 (usual ploughing, trench planting), whereas the accuracy for class 6 (corn?) is only 75.6%. Approximately 90% of regions are correctly classified in most classes. It is of interest to consider the error matrix (Table 5), which allow one to see the classes with erroneously classified data. Each row of the matrix is normalized to the number of correctly classified pixels in the corresponding classes. Regions from 5 to 18 are corn regions, and those from 36 to 53 are soya regions.

To find the error distribution in a particular class, we find the number of the class in the upper row of the table; the row with this number shows the percentage of pixels recognized as pixels of other classes whose numbers are indicated in the first column. The maximum error percentage values are of interest. At first glance, the maximum mutual errors could have been expected for classes characterized by different types of ploughing from north to south and from west to east. Nevertheless, this is not so, which follows from enumeration of all regions with more than 3% errors of referring to another class. The maximum error equal to 4.86% is referring of pixels of class 16 "corn — low-intrusive ploughing — north-south" to class 45 "soya beans — trench planting." The error of referring pixels of class 9 "corn — usual ploughing" to class 36 "soya beans" is equal to 3.65%. The error of referring pixels of class 41 "soya beans — usual ploughing — west-east" to class 6 "corn?" is 3.1%. The only logical (from the viewpoint of the ploughing direction) sufficiently large error of referring pixels of class 15 "corn — low-intrusive ploughing — west-east" to class 51 "soya beans — no ploughing — west-east" is equal to 2.98%.

CONCLUSIONS

Thus, it was experimentally demonstrated in the paper that transformation of the spectral components into the principal components and further spatial transformation by means of expansion of the principal components into empirical modes during classification of hyperspectral images ensures the formation of an effective system of recognition features. After neural network learning, the system offers a possibility of fine classification of hyperspectral images and ensures a high probability of correct classification of regions with similar spectral compositions, which are difficult to distinguish by usual methods.

The author is grateful to Dr. S. M. Borzov for useful comments.

This work was supported by the Ministry of Higher Education and Science of the Russian Federation (State Registration No. AAAA-A17-117052410034-6).

REFERENCES

1. *Promising Information Technologies of Remote Sensing of the Earth*, Ed. by V. A. Soifer (Novaya Tekhnika, Samara, 2015) [in Russian].
2. V. G. Bondur, "Advanced Approaches to Processing Large Fluxes of Hyperspectral and Multispectral Aerospace Information," Issled. Zemli iz Kosmosa, No. 1, 4–16 (2014).
3. A. V. Kuznetsov and V. V. Myasnikov, "Comparison of Algorithms of Controlled Elemental Classification of Hyperspectral Images," Komp. Optika **38** (3), 494–502 (2014).
4. V. A. Fursov, S. A. Bibikov, and O. A. Baida, "Topical Classification of Hyperspectral Images Based on the Conjugation Criterion," Komp. Optika **38** (1), 154–158 (2014).
5. S. M. Borzov, A. O. Potaturkin, O. I. Potaturkin, and A. M. Fedotov, "Analysis of the Efficiency of Classification of Hyperspectral Satellite Images of Natural and Man-Made Areas," Avtometriya **52** (1), 3–14 (2016) [Optoelectron., Instrum. Data Process. **52** (1), 1–10 (2016)].
6. S. M. Borzov and A. O. Potaturkin, "Efficiency of the Spectral-Spatial Classification of Hyperspectral Imaging Data," Avtometriya **53** (1), 32–42 (2017) [Optoelectron., Instrum. Data Process. **53** (1), 26–34 (2017)].
7. S. M. Borzov and A. O. Potaturkin, "Classification of Hyperspectral Images with Different Methods of Training Set Formation," Avtometriya **54** (1), 89–97 (2018) [Optoelectron., Instrum. Data Process. **54** (1), 76–82 (2018)].
8. S. M. Borzov and A. O. Potaturkin, "Spectral-Spatial Methods for Hyperspectral Image Classification. Review," Avtometriya **54** (6), 64–86 (2018) [Optoelectron., Instrum. Data Process. **54** (6), 582–599 (2018)].
9. E. S. Nezhevenko, A. S. Feoktistov, and O. Yu. Dashevskii, "Neural Network Classification of Hyperspectral Images on the Basis of the Hilbert–Huang Transform," Avtometriya **53** (2), 79–85 (2017) [Optoelectron., Instrum. Data Process. **53** (2), 165–170 (2017)].

10. *Lena. Material from Wikipedia*. https://ru.wikipedia.org/wiki/Lena_(image).
11. S. Beucher, "Geodesic Reconstruction, Saddle Zones and Hierarchical Segmentation," Image Anal. Stereol. **20** (2), 137–141 (2001).
12. L. Vincent, "Morphological Grayscale Reconstruction in Image Analysis: Applications and Efficient Algorithms," IEEE Trans. Image Process. **2** (2), 176–201 (1993).
13. J. C. Carr, W. R. Fright, and R. K. Beatson, "Surface Interpolation with Radial Basis Functions for Medical Imaging," in *Proc. of the Conf. ACM SIGGRAPH*, Los Angeles, USA, August 12–17, 2001, pp. 67–76.